Center for Turbulence Research
Proceedings of the Summer Program 2006

Auto-ignition and flame propagation effects in LES of burned gases diluted turbulent combustion

By P. Domingo†, L. Vervisch† AND D. Veynante‡

The impact of burned gases on flame stabilization is analyzed under the conditions of a laboratory jet-flame in vitiated coflow (Cabra *et al.* 2005). In this experiment, mass flow rate, temperature, and the exact chemical composition of hot products mixed with air sent toward the turbulent flame base are fully determined. Auto-ignition and partially premixed flame propagation are investigated for these operating conditions from simulations of prototype combustion problems using fully detailed chemistry. Using available instantaneous species and temperature measurements, *a priori* tests are performed to estimate the prediction capabilities of chemistry tabulations built from these archetypal reacting flows. The links between auto-ignition and premixed flamelets tables are discussed, along with the parameters controlling their low dimensional manifolds. Large-Eddy Simulation of the turbulent diluted jet flame is then performed, taking advantage of the observed self-similar behavior of the filtered chemical tables.

1. Introduction

Recirculating burned gases exist in most combustion systems where fuel and oxidizer are mixed with combustion products before they enter the main combustion zone. These recirculating hot products carry thermal energy that may help flame stabilization. They are also useful to dilute the reaction zones, which homogenizes the mixture and avoids the large temperature levels responsible for NOx emissions. In gas turbine combustion chambers, hot recirculating combustion products contribute to flame stabilization downstream of the swirled injection (Schneider *et al.* 2005). In car engines, Engine Gas Recirculation (EGR) is one of the studied options to control ignition in Homogeneous Charge Compression Ignition (HCCI) engines, there the chemical composition of the burned gases plays a key role (Subramanian *et al.* 2006). Burned gases are also present in furnaces, where they contribute to flame stability. For a high level of flame dilution by burned gases, the Moderate or Intense Low-oxygen Dilution (MILD) (Cavaliere & De Joannon 2004) or the Flameless regimes are observed (Tabacco *et al.* 2002). In the latter, very high dilution by burned gases leads to a strong decrease of temperature gradients followed by a dramatic reduction of NOx emission.

Accordingly, almost no practical combustion systems exist where recirculating burnt gases are not intimately involved in the process; they control part of the behavior of the turbulent reaction zones. The accurate control of recirculating hot products is now the main target of many design studies devoted to real combustion chambers. Nevertheless, so far, only a few studies have discussed dilution by burnt gases in the context of turbulent combustion modeling (Daly *et al.* 2005).

A variety of combustion regimes can be observed downstream of a non-premixed injection of reactants within recirculating burned products. The high temperature of the

† LMFN, CORIA - CNRS, Institut National des Sciences Appliquées de Rouen, France
‡ EM2C - CNRS, Ecole Centrale Paris, France

	Re	D (mm)	V (m/s)	T (K)	X_{O_2}	X_{N_2}	X_{H_2O}	X_{CH_4}
FUEL JET	28 000	4.57	100	320	0.15	0.52	0.0029	0.33
COFLOW	23 300	210	5.4	1 350	0.12	0.73	0.15	0.0003

TABLE 1. Conditions for the lifted methane-air jet flame in a vitiated coflow. Re: Reynolds number, D: Diameter, T: Temperature, X: Mole fraction, from Cabra *et al.* (2005).

gases can favor auto-ignition, the partial premixing of fuel with oxidizer can lead to the development of partially premixed flame propagation and, further downstream, diffusion flame burning is likely to develop. Chemistry tabulation is discussed for these various regimes in the context of Large-Eddy Simulation (LES). Links between the *a priori* distinct auto-ignition, premixed, and diffusion flamelets low dimensional manifolds are evidenced for the operating conditions of the lifted methane-air jet flame in a vitiated coflow experiment reported by Cabra *et al.* (2005). Subsequently, this chemistry tabulation is combined with Presumed Conditional Moment (PCM) Sub-Grid Scale (SGS) modeling (Vervisch *et al.* 2004, Domingo *et al.* 2005) to perform LES of the turbulent lifted jet flame in a vitiated stream.

2. Auto-ignition and flame propagation in a diluted jet flame

2.1. *Conditions of the Cabra et al. experiment*

The exact chemical composition and mass flow rate of recirculating burnt gases are often difficult to accurately calibrate and measure in real combustion chambers. To gain greater understanding of flame stabilization in environments where burnt gases dominate, Cabra *et al.* (2005) designed a laboratory vitiated burner in which the injection conditions of reactants and hot products are fully determined. In addition to detailed scalar measurements, Reynolds-Average Navier-Stokes (RANS) calculations were also reported in Cabra *et al.* (2005). The burner consists of a round fuel jet issuing into a coflow of hot combustion products. This vitiated stream is obtained from hydrogen/air lean premixed combustion (equivalence ratio $\phi = 0.4$) and it is mainly composed of H_2O and air flowing at 1350 K. The central fuel jet mixture is composed of 33% CH_4 and 67% air, by volume (equivalence ratio $\phi = 4.4$). The bulk velocity of the fuel jet and of the coflow velocity are of the order of 100 m/s and 5.4 m/s respectively. The geometry of the burner and the operating conditions are summarized in Table 1. This burner configuration was first used to study H_2/N_2 jet flame in vitiated coflow (Cabra *et al.*, 2002).

2.2. *Auto-ignition and flame propagation in diluted combustion*

Various flame propagation scenarios have been discussed to explain experimental and numerical observations of lifted flame stabilization in the case of gaseous and spray injection, with or without swirl (Muñiz & Mungal 1997, Marley *et al.* 2000, Sommerer *et al.* 2004, Domingo & Vervisch 2006). Flame stabilization was attributed to the existence of more or less distorted partially premixed fronts interacting with turbulence and propagating against the incoming flow. In the presence of hot products, the reactants are partially premixed with gases that bring additional energy that can help with flame stabilization, mainly through thermal effects that reduce the auto-ignition delay, increase flame speed and diminish flame sensitivity to quenching. These effects may be counterbalanced when too much of diluent is mixed with the reactants, then the reaction zones

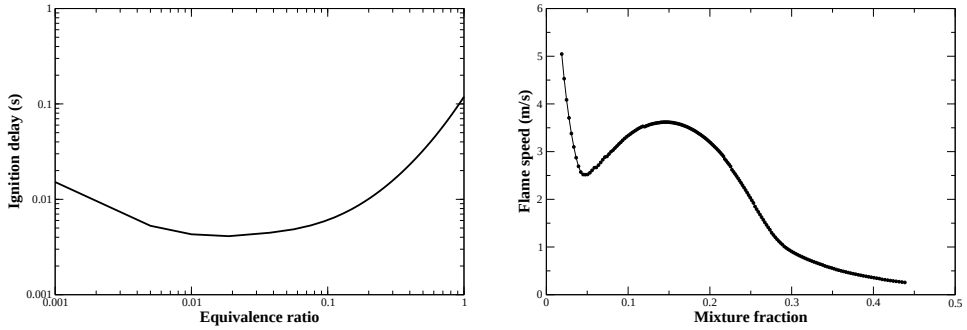

FIGURE 1. Left: Ignition delay versus equivalence ratio. Right: Flame speed versus mixture fraction.

development is reduced because of the additional presence of thermal ballast and the lack of reactivity of the highly diluted mixture. In the Cabra *et al.* experiment, the fresh reactants issuing from the central jet are mixed with hot product (H_2O) and air before the turbulent flame base develops, somewhere between X/D = 30 and 40. X denotes the vertical axis of the burner and D the diameter of the fuel jet (Table 1). Upstream of the flame base, scalars (temperature, species concentrations) follow a response of the form $\varphi_m(Z) = Z\varphi_{F,o} + (1-Z)\varphi_{O,o}$, where Z is the mixture fraction, the subscripts $_{F,o}$ and $_{O,o}$ denote a quantity in pure fuel or vitiated streams respectively ($Z_{F,o} = 1$ and $Z_{O,o} = 0$). The stoichometric point is located at $Z_s = 0.1769$. For every mixture fraction ranging between the flammability limits, a set of diluted reactants φ_i are generated. Ignition delays and freely propagating premixed flames are subsequently computed for these conditions, chemistry is described with the 49 species detailed in the GRI 3.0 methane-air mechanism (http://www.me.berkeley.edu/gri-mech/), SENKIN and PREMIX (Kee *et al.* 1992) softwares have been used with complex transport properties. The results are collected in two chemical tables, $Y_i^{AI}(Z,t)$ for the perfectly mixed reactors, used to compute autoignition delays, and $Y_i^{PF}(Z,x)$ for premixed flamelets; t is the time coordinate in the reactor and x the position through the premixed flame. The Flame Prolongation of Intrinsic low dimensional manifold (FPI) method is adopted (Giquel *et al.* 2000), the tables are reorganized with the progress of reaction $Y_c(Z,\xi) = Y_{CO}(Z,\xi) + Y_{CO_2}(Z,\xi)$, where ξ denotes either time or position. By eliminating the ξ coordinate between $Y_i(Z,\xi)$ and $Y_c(Z,\xi)$, two-dimensional manifolds capturing autoignition and flame propagation are obtained:

$$Y_i^{AI}(Z,Y_c) \;\; ; \;\; Y_i^{PF}(Z,Y_c) \tag{2.1}$$

Figure 1 (left) shows the smallest values of ignition delay versus equivalence ratio $\phi = Z(1-Z_s)/[Z_s(1-Z)]$. A minimum value of this delay of the order of 4 ms is found for $\phi \approx 0.02$ ($Z \approx 0.00427$); these observations are similar to these reported by Cabra *et al.* (2005). Autoignition delays rapidly increase for equivalence ratio above unity. Therefore autoignition is more likely to contribute to stabilization on the very lean side of the axisymmetric mixing layer. This implies constraints for simulations of such vitiated combustion problems. For fixed boundary conditions (chemical gas compositions and vitiated stream temperature) and fixed chemical scheme, small variations in the description of mixing on the lean side would be accompanied by large variations of ignition delay, which

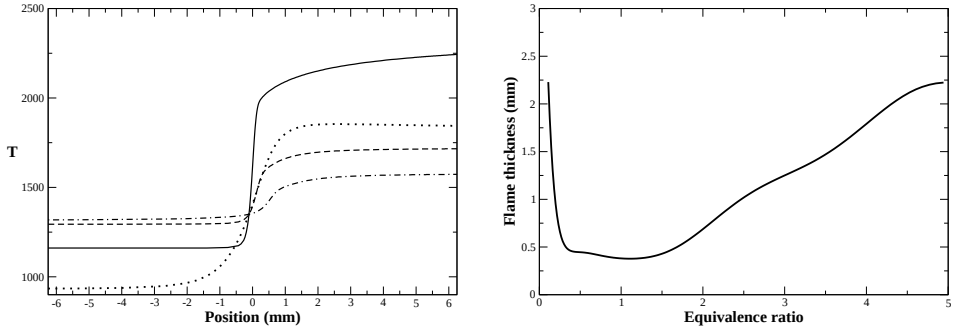

FIGURE 2. Left: Temperature profiles through representative premixed flames. Solid line: $\phi = 1$. Dash line: $\phi = 0.27$. Dotted dash line: $\phi = 0.16$. Dotted line: $\phi = 3.16$. Right: Characteristic flame thickness.

may strongly impact the turbulent flame base streamwise location. It is therefore crucial in the simulations to carefully capture the mixing up to the mixture fraction points that are well below the stoichiometric value. The LES mesh resolution needs to be kept sufficiently high when approaching the vitiated coflow stream and the overall accuracy of the numerical scheme used to transport scalars should be high enough.

The flame speed response to mixture fraction is plotted in fig. 1 (right). For $Z > 0.1$, it features a usual shape with a maximum level of 3.6 m/s in the vicinity of the stoichiometric condition. On the lean side, however, the speed increases mostly as a result of the high temperature of the vitiated stream. Solutions for premixed flame propagation exist up to $Z \approx 0.02$ ($\phi \approx 0.1$), with a flame speed of the order of 5 m/s. The temperature increase becomes very small for these lean flames, as shown in fig. 2 (left). Nevertheless, it can be anticipated that flame propagation may also promote flame stabilization on the lean mixture iso-surfaces, since the coflow maximum velocity (5.4 m/s) is of the same order as the lean maximum flame speed. This may occur when autoignition was not successful due to local flow conditions, or just after autoignition has initiated combustion. A measure of the reaction zone thickness, δ_L, may be evaluated for each equivalence ratio from the maximum gradient of Y_c in the unstretched laminar flame $\delta_L = {Y_c}^{Eq} / \max(dY_c/dx)$, where ${Y_c}^{Eq}$ is the equilibrium condition of the progress of reaction (see fig. 2 right). The dilution by hot products contributes to an increase of the characteristic reaction zone thickness on the lean side, where autoignition delays are small and the flame speeds large. With chemistry tabulated from the relations 2.1, to fully resolve the Y_c signal describing the reaction zones, the mesh resolution $h \approx \delta_L/10$ must be between $h < 0.03$ mm and $h < 0.2$ mm, depending on the local equivalence ratio. Notice that much thinner (more than an order of magnitude smaller) radical layers are embedded within the Y_c signal. These would need to be resolved in fully detailed chemistry simulations of this jet flame.

2.3. *A priori tests of chemistry tabulation from experiments*

Single-point species concentration measurements are available for the Cabra et al. (2005) experiment (http://www.me.berkeley.edu/cal/VCB/Data/VCMAData.html). The instantaneous measured values of $Y_c = Y_{CO} + Y_{CO_2}$ (using CO LIF) and Z are used to construct chemical flame structures from $Y_i^{AI}(Z, Y_c)$ and $Y_i^{PF}(Z, Y_c)$, the autoignition and pre-

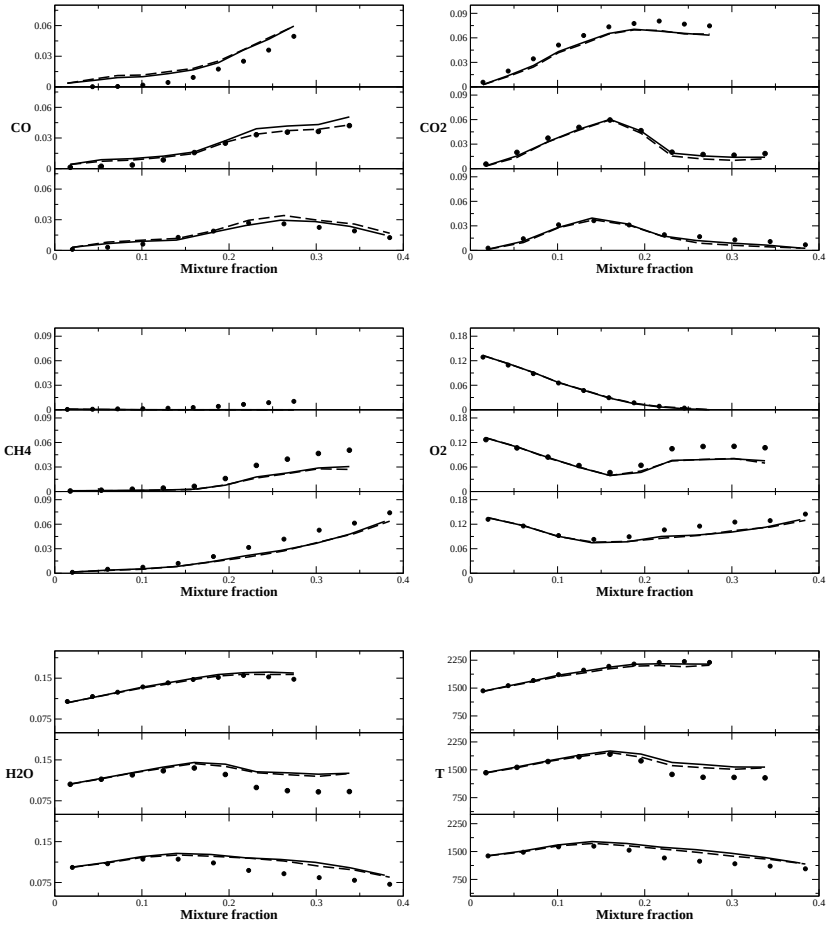

FIGURE 3. Conditional mean versus mixture fraction, *a priori* tests from measurements. Left column from top to bottom: CO, CH_4, H_2O mass fractions. Right column: CO_2, CH_4, temperature. Symbols: Measurements. Solid Line: FPI database. Dashed Line: Autoignition database. From bottom to top, streamwise position X/D = 40, 50, 70.

mixed flamelet chemical tables (Eq. 2.1). From every single-point measurement, Z and Y_c are extracted and then enter the tables to get Y_i^{AI} and Y_i^{PF}. For every point of the measurements, three values of Y_i are then available, one from the measurements and two from the tables. Conditional means are computed as averages of those points for a given bin in Z. The comparison of $\langle Y_i^{AI}|Z^*\rangle$ and $\langle Y_i^{PF}|Z^*\rangle$, the resulting conditional means versus mixture fraction, with their measured values provides a direct *a priori* test of such chemistry tabulation. The results are shown in fig. 3, where it is seen that responses from autoignition and premixed flamelets tables are very close. The flame structure in mixture fraction space is well captured on the lean side. On the rich side, the tabulated responses deviate from the measurements. Part of this deviation may be attributed to the appearance of diffusion flame effects leading to fluxes in mixture fraction space that are not included in the chemical tables (Fiorina *et al.* 2005). Far downstream (X/D = 70),

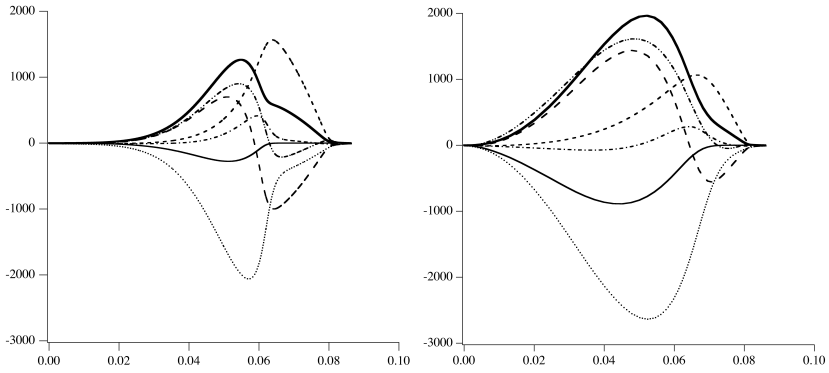

FIGURE 4. Reaction rates of various species plotted versus the progress variable mass fraction $Y_c = Y_{CO} + Y_{CO_2}$: $\dot{\omega}_c$ (———); $\dot{\omega}_{CH_4}$ (———); $\dot{\omega}_{O_2}$ (·····); $\dot{\omega}_{CO_2}$ (– – – –); $\dot{\omega}_{CO}$ (— — —); $\dot{\omega}_{H_2O}$ (— ·· —); $\dot{\omega}_{OH}$ (— · —). Left: auto-ignition; right: freely propagating one-dimensional premixed flame. Mixture fraction $Z = 0.149$. Reaction rates are given in s^{-1}. At the location where χ_{Y_c} reaches its maximum, $\dot{\omega}^{PF}_{CH_4}/\chi_{Y_c} \approx 200$ (see relations 3.2).

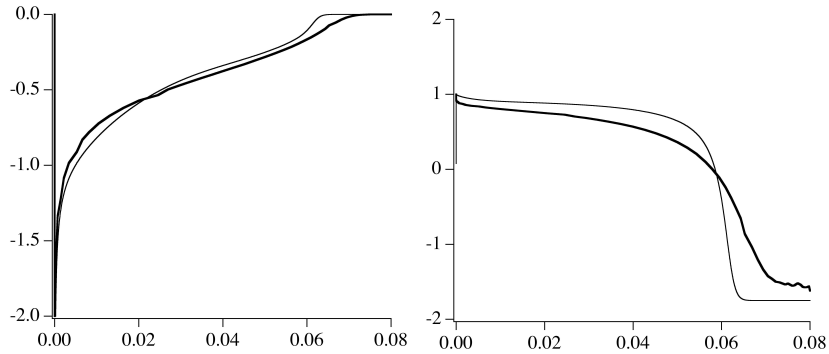

FIGURE 5. Comparison of $\partial Y_k/\partial Y_c$ in the auto-ignition (———) and the propagation (———) databases for methane (CH_4, left) and carbon monoxide (CO, right). Conditions are the same as in fig. 4.

where diffusion flame burning may be expected to dominate, the deviation from measurements is also apparent on the lean side. Conclusions from these preliminary apriori tests indicate that the turbulent flame base can be approximated with a combination of autoignition and premixed flamelet chemical tables, but a more careful analysis would be required to capture the flame further downstream.

3. Linking auto-ignition and flame propagation in low-dimensional manifolds

For a fixed value of the mixture fraction Z^o, the low-dimensional manifolds, $Y_i^{AI}(Z^o, Y_c)$ and $Y_i^{PF}(Z^o, Y_c)$, describing autoignition and premixed flamelets are controlled by the balance equations

$$\rho \frac{\partial Y_i^{AI}}{\partial t} = \rho \dot{\omega}_i^{AI} \quad ; \quad \rho_0 S_L \frac{\partial Y_i^{PF}}{\partial x} = \frac{\partial}{\partial x}\left(\rho \mathcal{D} \frac{\partial Y_i^{PF}}{\partial x}\right) + \rho \dot{\omega}_i^{PF} \tag{3.1}$$

where usual notations are adopted. From the relations $\nabla Y_i = (\partial Y_i/\partial Y_c)\nabla Y_c$ and $\nabla^2 Y_i = (\partial^2 Y_i/\partial Y_c^2)|\nabla Y_c|^2 + (\partial Y_i/\partial Y_c)\nabla^2 Y_c$, and eliminating Y_c budgets (Eqs 3.1 applied to Y_c),

the relations 3.1 may be reorganized as:

$$\dot{\omega}_c^{AI}\frac{\partial Y_i^{AI}}{\partial Y_c}=\dot{\omega}_i^{AI} \quad ; \quad \dot{\omega}_c^{PF}\frac{\partial Y_i^{PF}}{\partial Y_c}=\dot{\omega}_i^{PF}+\chi_{Y_c}\frac{\partial^2 Y_i^{PF}}{\partial Y_c^2} \tag{3.2}$$

where $\chi_{Y_c}=\mathcal{D}|\nabla Y_c|^2$ is the scalar dissipation rate of Y_c measured in the premixed flamelets. These last relations show that differences between the tables occur in the molecular diffusion term, expressed in terms of the scalar dissipation rate in Eq. 3.2. This point is illustrated in fig. 4, where reaction rates of various species are displayed versus Y_c. The two responses mainly differ in the burnt gas region, which is larger in the phase space for auto-ignition ($Y_c \geq 0.06$) than for premixed flame ($Y_c \geq 0.07$). Because of molecular diffusion, absent in homogeneous auto-ignition, products and heat diffuse toward fresh gases in premixed flames, modifying the hot burnt zone. Note also that the OH reaction rate is always positive for auto-ignition whereas this radical, transported by molecular diffusion, is consumed on the fresh gas side of premixed flames. Despite these differences observed on chemical sources, the slopes $\partial Y_i/\partial Y_c$ measured in the two manifolds stay very close for major species and $(\partial Y_i/\partial Y_c)^{AI} \approx (\partial Y_i/\partial Y_c)^{PF}$ as shown in fig. 5 for methane and carbon monoxide. Combining the relations 3.2 with the assumption that slopes stay very close creates a direct link between the two low-dimensional manifolds used to simulate the Cabra *et al.* (2006) experiment:

$$\rho\dot{\omega}_i^{AI}=\frac{\dot{\omega}_c^{AI}}{\dot{\omega}_c^{PF}}\left[\rho\chi_{Y_c}\frac{\partial^2 Y_i^{PF}}{\partial Y_c^2}+\rho\dot{\omega}_i^{PF}\right] \tag{3.3}$$

Figure 6 compares autoignition sources estimated from their direct tabulation and from Eq. 3.3. An interesting agreement is obtained for main species such as methane and carbon monoxide. Some of these observations are now used for LES of lifted flame in vitiated coflow.

4. LES of a turbulent diluted jet-flame

The SGS flame structure may be approximated using PCM, a closure based on beta-shape presumed probability density function initially formulated in a RANS context (Vervisch *et al.* 2004), then extended to LES of premixed turbulent combustion (Domingo *et al.* 2005). Filtered scalars and sources may be cast in the form:

$$\widetilde{\varphi}(\underline{x},t)=\int_0^1\left(\overline{\varphi|Z^*;\underline{x},t}\right)\widetilde{P}(Z^*;\underline{x},t)\,dZ^* \tag{4.1}$$

From the above analysis, combustion is likely to begin with autoignition, and rapidly followed by flame propagation. But when autoignition cannot initially occur, flame propagation may also be the stabilizing mechanism. The conditional filtered means $\left(\overline{\varphi|Z^*;\underline{x},t}\right)$ must be organized to capture this peculiar structure of the lifted flame in mixture fraction space. Accounting for these observations and for the fact that chemical tables are almost the same for low levels of the progress of the reaction, it is proposed to approximate $\left(\overline{\varphi|Z^*;\underline{x},t}\right)$ from the autoignition and premixed flamelet tables according to

$$\left(\overline{\varphi|Z^*;\underline{x},t}\right)=(1-\overline{c})\int_0^1\varphi^{AI}(Z^*,c^*)\overline{P}(c^*;\underline{x},t)dc^*+\overline{c}\int_0^1\varphi^{PF}(Z^*,c^*)\overline{P}(c^*;\underline{x},t)dc^* \tag{4.2}$$

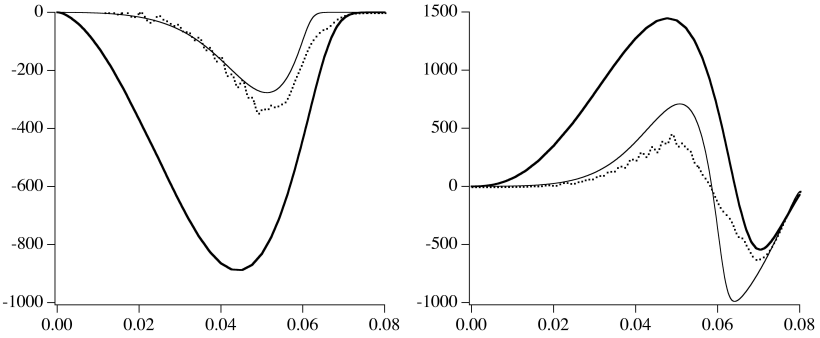

FIGURE 6. Comparison of auto-ignition (———), propagation (▬▬▬), and reconstructed ignition (····· , Eq. 3.3) reaction rates for methane (CH_4, left) and carbon monoxide (CO, right). Conditions are the same as in fig. 4. $\mathcal{D}$ is assumed constant.

where $c = Y_c/Y_c^{Eq}$ is a progress variable. Mixture fraction and progress variables are assumed independent (notice that this applies to c that is a normalized quantity, but not to the progress of reaction Y_c or to any other quantity $\varphi = Y_i$ of the tables, Vervisch *et al.*, 2004). Then, $\overline{c} = \overline{\rho Y}_c/\overline{\rho Y}_c^{Eq}$ and $c_v = Y_{c_v}/\widetilde{Y_c^{Eq^2}} + \widetilde{Y}_c^{\,2}(1/\widetilde{Y_c^{Eq^2}} - 1/\widetilde{Y_c^{Eq}}^{\,2})$, where $c_v = \overline{cc} - \overline{c}\,\overline{c}$ and $Y_{cv} = \widetilde{Y_c Y_c} - \widetilde{Y}_c\,\widetilde{Y}_c$ denote SGS variances. For these first simulations, the basic algebraic closure $\overline{\rho} Y_{cv} = C_v \overline{\rho}\Delta^2 |\nabla \widetilde{Y}_c|^2 + C_v(\Delta^2 Sc_T/\nu_T)(\widetilde{\dot{\omega}_{Y_c} Y_c} - \widetilde{\dot{\omega}}_{Y_c}\widetilde{Y}_c)$ is chosen for the SGS variance of the progress of the reaction, with C_v =1.5 and $Sc_T = 0.6$ (Domingo *et al.* 2005). Other quantities necessary to presume the PDFs, $\widetilde{Z}$, Z_v, and $\widetilde{Y}_c$ are obtained from their balance equations:

$$\frac{\partial \overline{\rho}\widetilde{Z}}{\partial t} + \nabla \cdot \overline{\rho}\widetilde{\mathbf{u}}\widetilde{Z} = -\nabla \cdot \overline{\tau}_Z + \nabla \cdot \left(\overline{\rho}\mathcal{D}\nabla \widetilde{Z}\right) \tag{4.3}$$

$$\frac{\partial \overline{\rho} Z_v}{\partial t} + \nabla \cdot \overline{\rho}\widetilde{\mathbf{u}} Z_v = -\nabla \cdot \overline{\tau}_{Z_v} + \nabla \cdot \left(\overline{\rho}\mathcal{D}\ \nabla \widetilde{Z}_v\right) - 2\overline{\tau}_{Z_v} \cdot \nabla \widetilde{Z} - 2\overline{s}_{\chi Z} \tag{4.4}$$

$$\frac{\partial \overline{\rho}\widetilde{Y}_c}{\partial t} + \nabla \cdot \overline{\rho}\widetilde{\mathbf{u}}\widetilde{Y}_c = -\nabla \cdot \overline{\tau}_{Y_c} + \nabla \cdot \left(\overline{\rho}\mathcal{D}\ \nabla \widetilde{Y}_c\right) + \overline{\rho}\widetilde{\dot{\omega}}_{Y_c} \tag{4.5}$$

The SGS turbulent fluxes, $\overline{\tau}_Z$, $\overline{\tau}_{Z_v}$, and $\overline{\tau}_{Y_c}$ are expressed using the filtered structure function closure of Lesieur *et al.* (2005). The SGS scalar dissipation rate is modeled as $\overline{s}_{\chi Z} = \overline{\rho} Z_v/(\Delta^2 \nu_T)$, where Δ is the characteristic filter size and ν_T is the SGS eddy viscosity given by filtered structure function modeling. The filtered sources of progress of reaction $\widetilde{\dot{\omega}}_{Y_c}$ and of energy are analytically expressed from the relations 4.1 and 4.2, as discussed in the next section.

The set of Navier-Stokes equations in their fully compressible form are solved together with above equations. A fourth-order finite volume skew-symmetric-like scheme proposed by Ducros *et al.* (2000) is adopted for the spatial derivatives. This scheme was specifically developed for LES and is combined here with second-order Runge Kutta explicit time stepping. Acoustic waves are included in the fully compressible formulation and Navier-Stokes characteristic boundary conditions are retained (Poinsot & Lele 1992). The mesh is composed of 2150,000 nodes with a characteristic mesh size h that verifies 0.3 mm $< h <$ 2.5 mm. Its spanwise and streamwise lengths are 28D and 90D respectively. Turbulence is generated in the inlet plane following the procedure proposed by Klein *et al.* (2002).

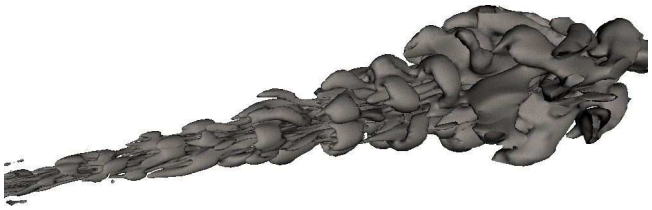

FIGURE 7. Snapshot iso-Q for Q= $V_F/2D$, V_F is the fuel jet bulk velocity.

4.1. *Self-similar SGS chemistry tabulation*

As discussed by Naudin *et al.* (2006), the self-similarity behavior of laminar premixed flames evidenced by Ribert *et al.* (2006) may be extended to turbulent flames. The mean, or filtered, reaction rate of species is then split into two categories of contributions related to the reactants mixing ($\widetilde{Z}, Z_v$) and to the progress of reaction ($\overline{c}, c_v$). This decomposition was found valid for both, autoignition and premixed flame propagation. The filtered burning rate may be written:

$$\widetilde{\dot{\omega}}_c^{\alpha} \approx \max[\dot{\omega}_c]^{\alpha} \mathcal{F}_c^{\alpha}(\overline{c}, S_c) \mathcal{G}_c^{\alpha}(\widetilde{Z}, S_Z) \tag{4.6}$$

where α denotes either "AI" for the autoignition table or "PF" for the premixed flamelet tabulation. $S_c = c_v/(\overline{c}(1-\overline{c}))$ and $S_Z = Z_v/(\widetilde{Z}(1-\widetilde{Z}))$ are the unmixedness of the reaction progress variable and the mixture fraction. The functions $\mathcal{F}_c^{\alpha}$ and $\mathcal{F}_c^{\alpha}(\overline{c}, S_c)$ read

$$\begin{aligned}\mathcal{F}_c^{AI}(\overline{c}, S_c) = A_c^{AI}(s_c) \big[\overline{c}^{\, b_c^{AI}(s_c)} (1-\overline{c})^{c_c^{AI}(s_c)} + \min\left(\overline{c}, d_c^{AI}(s_c)\right) \\ + \min\left(1-\overline{c}, d_c^{AI}(s_c)\right) - d_c^{AI}(s_c) \big]\end{aligned} \tag{4.7}$$

$$\mathcal{G}_c^{AI}(\widetilde{Z}, S_Z) = A_z^{AI}(s_Z)\, \widetilde{Z}^{\, b_Z^{AI}(s_Z)} \left(1-\widetilde{Z}\right)^{c_Z^{AI}(s_Z)} \tag{4.8}$$

$$\mathcal{F}_c^{PF}(\overline{c}, S_c) = A_c^{PF}(s_c)\, \overline{c}^{\, b_c^{PF}(s_c)} (1-\overline{c})^{c_c^{PF}(s_c)} \tag{4.9}$$

$$\mathcal{G}_c^{PF}(\widetilde{Z}, S_Z) = A_Z^{PF}(s_Z)\, \widetilde{Z}^{\, b_Z^{PF}(s_Z)} \left(1-\widetilde{Z}\right)^{c_Z^{PF}(s_Z)} \tag{4.10}$$

With these equations, source term databases are reduced from four-dimensional matrixes, depending on $\widetilde{c}$, c_v, $\widetilde{Z}$, and Z_v, to thirteen vectors (A_c^{AI}, A_z^{AI}, A_c^{PF}, A_Z^{PF}, b_c^{AI}, c_c^{AI}, d_c^{AI}, b_z^{AI}, c_z^{AI}, b_c^{PF}, c_c^{PF}, b_z^{PF}, c_z^{PF}) discretized on twenty values of segregation factors, saving a significant amount of memory, a point of major importance on massively parallel machines. Simulations reported below have been performed using this self-similar SGS chemistry tabulation. The exact values of the various parameters and functions are not given here due to space restrictions, but they can be provided upon request.

4.2. *LES results*

The development of the turbulent jet is shown in fig. 7, which displays iso-surface of one positive value of $Q = -0.5(\partial\widetilde{u}_i/\partial x_j)(\partial\widetilde{u}_j/\partial x_i)$, a quantity useful to detect resolved coherent structures (Hunt *et al* 1988). A transverse cut of the burning rate at X = 52D is shown in fig. 8 (left), with two iso-mixture fraction lines corresponding to the position of the stoichiometric surface and the maximum flame velocity. At this location, combustion mainly occurs along the stoichiometric surface, with the maximum flame velocity mixture ($Z = 0.02$) bordering the reaction zone. The jet centerline average, $< \widetilde{T} >$, and fluctuations, $< \widetilde{T}\widetilde{T} > - < \widetilde{T} >< \widetilde{T} >$, of temperature suggest that the

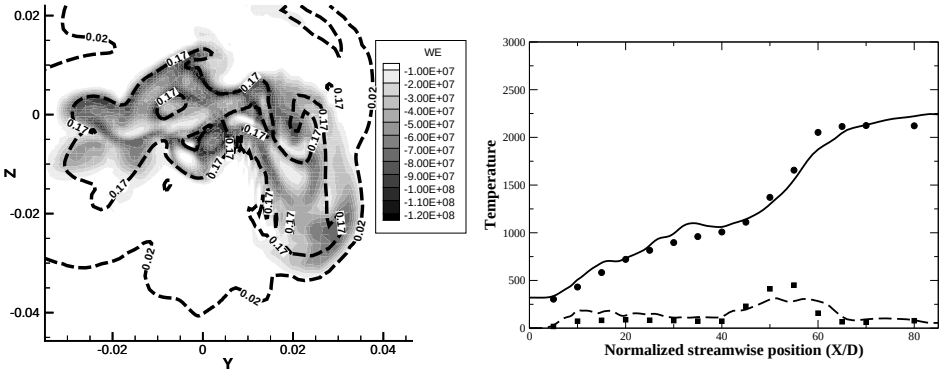

FIGURE 8. Left: Transverse cut at X = 52D, dashed line: Iso-mixture fraction line for $Z_s = 0.177$ and $Z = 0.02$. Flood: Burning rate (J/(m^{3}s)). Right: Profile of average (line and circle) and RMS (dash line and square) temperature on the centerline of the jet. Symbols: Measurements. Line: LES.

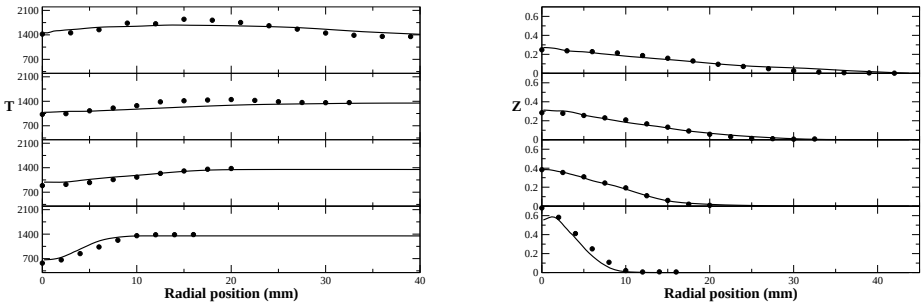

FIGURE 9. Radial profiles of average temperature (left) and mixture fraction (right). Symbol: Measurements. Solid-line: LES. From bottom to top, streamwise position X/D = 15, 30, 40, 50.

turbulent flame base position is well captured (fig. 8-right). These quantities have been averaged over 4 flow times (measured from average inlet velocity and streamwise length of the computational domain). Radial profiles of mean temperature and mixture fraction are averaged in both time and space using the axi-symmetric character of the flow and compared to measurements in fig. 9. Most of the mean flame structured is reproduced. Conditional means in mixture fraction space are constructed from LES results (see fig. 10. The temperature and CO responses are reproduced at the flame base, but the CO mass fraction is over-estimated at X = 70D. This could be attributed to diffusion flame burning (among other possible causes associated with chemistry description), confirming the need for accounting for diffusion flame behavior downstream of the turbulent flame base.

5. Conclusion

The impact of burnt gases on flame stabilization has been studied using autoignition and premixed flamelet chemistry tabulations under the operating conditions of a labo-

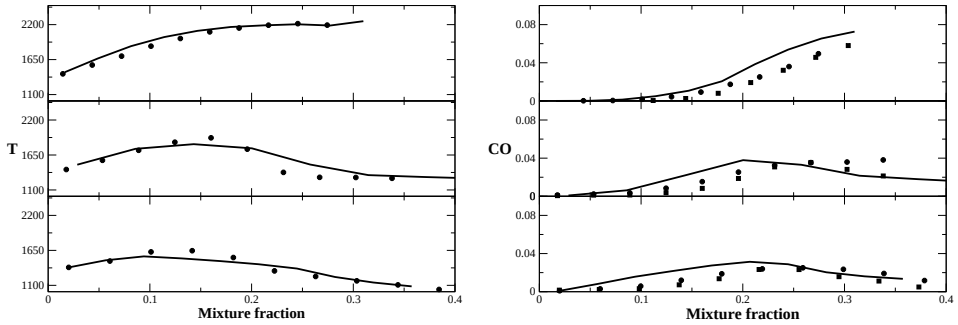

FIGURE 10. Conditional mean versus mixture fraction. Symbol: Measurements (instantaneous quantity). Solid-line: LES (filtered quantity). Left: Temperature. Right: CO mass fraction, circle: LIF, square Raman. From bottom to top, streamwise position X/D = 40, 50, 70.

ratory lifted jet flame in vitiated coflow. LES using a combination of these tabulations was found to reproduce most of the major chemical properties of this flame. In future work, the detailed structure of the flame base will be further analyzed from these simulations in the light of the links that were evidenced between the autoignition and premixed flamelets chemical tables.

Acknowledgment

The authors have benefited from stimulating discussions with the members of the CTR Summer Program Combustion Group.

REFERENCES

CABRA, R., CHEN, J. Y., DIBBLE, R. W., KARPETIS, A. N. & BARLOW, R. S. 2005 Lifted methane-air jet flame in vitiated coflow. *Combust. Flame* **143** (4), 491–506.

CABRA, R., MYHRVOLD, T., CHEN, J.-Y., DIBBLE, R. W., KARPETIS, A. N. & BARLOW, R. S. 2002 Simultaneous Laser Raman-Rayleigh-LIF measurements and numerical modeling results of a lifted turbulent H2/N2 jet flame in a vitiated coflow. *Proc. Combust. Inst.* **29**, 1881–1888.

CAVALIERE, A. & DE JOANNON, M. 2004 Mild combustion. *Progress in Energy and Combustion Sciences* **30** (4), 329–366.

DALY, B. B., RIESMEIER, E. & PETERS, N. 2005 Effect of fuel mixture on moderate and intense low oxygen dilution combustion. *Combust. Flame* **137**.

DOMINGO, P. & VERVISCH, L. 2006 DNS of partially premixed flame propagating in a turbulent rotating flow. *Proc. Combust. Inst.* **31**.

DOMINGO, P., VERVISCH, L., PAYET, S. & HAUGUEL, R. 2005 DNS of a premixed turbulent V-flame and LES of a ducted-flame using a FSD-PDF subgrid scale closure with FPI tabulated chemistry. *Combust. Flame* **143** (4), 566–586.

DUCROS, F., LAPORTE, F., SOULÈRES, T., GUINOT, V., MOINAT, P. & CARUELLE, B. 2000 High-order fluxes for conservative skew-symmetric-like schemes in structured meshes: application to compressible flows. *J. Comp. Phys.* **161**, 114–139.

Fiorina, B., Gicquel, O., Vervisch, L., Darabiha, N. & Carpentier, S. 2005 Approximating the chemical structure of partially premixed and diffusion counterflow flames using fpi flamelet tabulation. *Combust. Flame* **140** (3), 147–160.

Gicquel, O., Darabiha, N. & Thevenin, D. 2000 Laminar premixed hydrogen / air counterflow flame simulations using flame prolongation of ildm with differential diffusion. *Proc. Comb. Inst.* **28**, 1901–1908.

Hunt, J. C. R., Wray, A. A. & Moin, P. 1988 *Eddies, stream, and convergence zones in turbulent flows*. Annual Research Briefs, Center for Turbulence Research, Stanford.

Kee, R. J., Grcar, J. F., Smooke, M. D. & Miller, J. A. 1992 A fortran program for modeling steady laminar one-dimensional premixed flames. *Tech. Rep.*. Sandia National Laboratories.

Klein, M., Sadiki, A. & Janicka, J. 2002 A digital filter based generation of inflow data for spatially developing direct numerical or large eddy simulations. *J. Comp. Physics* (186), 652–665.

Lesieur, M., Métais, O. & Comte, P. 2005 *Large-Eddy Simulations of Turbulence*. Cambridge University Press, Cambridge UK.

Marley, S. K., Lyons, K. M. & Watson, K. A. 2004 Leading-edge reaction zones in lifted-jet gas and spray flames. *Flow Turbulence and Combustion* **72** (1), 29–47.

Muñiz, L. & Mungal, M. G. 1997 Instantaneous flame-stabilization velocities in lifted-jet diffusion flames. *Combust. Flame* **111** (1/2), 16–31.

Naudin, A., Fiorina, B., Paubel, X., Veynante, D. & Vervisch, L. 2006 *Self-similar behavior of chemistry tabulations in laminar and turbulent multi-fuel injection combustion systems*. Proceedings of the Summer Program, Center for Turbulence Research, Stanford.

Poinsot, T. & Lele, S. K. 1992 Boundary conditions for direct simulations of compressible viscous flows. *J. Comp. Phys.* **1** (101), 104–129.

Schneider, C., Dreizler, A. & Janicka, J. 2005 Fluid dynamical analysis of atmospheric reacting and isothermal swirling flows. *Flow, Turbulence and Combustion* **74** (1), 103–127.

Sommerer, Y., Galley, D., Poinsot, T., Ducruix, S. & Veynante, S. 2004 Les of flashback and extinction in a swirled burner. *J. of Turbulence* **5** (1).

Subramanian, G., Bounaceur, R., Cruz, A. P. & Vervisch, L. 2006 Chemical impact of co and h2 addition on the auto-ignition delay of homogeneous n-heptane/air mixtures. *Combust. Sci. Tech. In press* .

Tabacco, D., Innarella, C. & Bruno, C. 2002 Theoretical and numerical investigation on flameless combustion. *Combust. Sci. Tech.* **174**.

Vervisch, L., Hauguel, R., Domingo, P. & Rullaud, M. 2004 Three facets of turbulent combustion modelling: DNS of premixed V-flame, LES of lifted nonpremixed flame and RANS of jet-flame. *J. of Turbulence* **5** (4), 1–36.